minerals

Article

Palaeoweathering Conditions, Provenance, and Tectonic Setting of the Early Silurian Longmaxi Formation in the Upper Yangtze Region (Southern China): Evidence from Geochemistry

Liang Zhao [1], Yong Li [2,*], Chengjie Zou [3], Shaoze Zhao [3] and Chaorong Wu [2]

1 College of Energy, Chengdu University of Technology, Chengdu 610059, China; zhao_liang@stu.cdut.edu.cn
2 College of Geophysics, Chengdu University of Technology, Chengdu 610059, China
3 College of Earth Sciences, Chengdu University of Technology, Chengdu 610059, China
* Correspondence: liy@cdut.edu.cn

Abstract: The Longmaxi-1 black shales in the Upper Yangtze region are a vital source rocks in southern China. This study investigates the palaeoweathering conditions, provenance, and tectonic setting of the Longmaxi-1 black shale from an elemental geochemical perspective, ultimately revealing its tectonic setting. The results showed that the Longmaxi-1 black shales in the sedimentary period have the characteristics of primary deposition. The Longmaxi-1 black shales were deposited as a primary deposition under a mainly humid climate. However, fluctuations in climatic conditions were recorded from the bottom to the upper part of the formation. The parent rock of the Longmaxi-1 black shales in the Upper Yangtze region is a mixture provenance, mainly composed of intermediate-acid volcanic lithologies (granite and granodiorite), followed by mature quartzite and basalt. Black shale deposition is related to the tectonic setting of active continental margin and island arc-continent collision. The Cathayian orogenic belts and the North Qiangling orogenic belt may have played a role in the genesis of the Longmaxi-1 black shales within the Upper Yangtze region. This study provides significant clues regarding the reconstruction of the palaeoclimatic and palaeogeographical conditions of the Upper Yangtze region during the Early Silurian period.

Keywords: Upper Yangtze region; Longmaxi-1 black shale; provenance analysis; elemental geochemistry

check for updates

Citation: Zhao, L.; Li, Y.; Zou, C.; Zhao, S.; Wu, C. Palaeoweathering Conditions, Provenance, and Tectonic Setting of the Early Silurian Longmaxi Formation in the Upper Yangtze Region (Southern China): Evidence from Geochemistry. *Minerals* **2023**, *13*, 576. https://doi.org/10.3390/min13040576

Academic Editor: Stavros Kalaitzidis

Received: 4 February 2023
Revised: 14 April 2023
Accepted: 18 April 2023
Published: 20 April 2023

1. Introduction

Provenance analysis links the study of sedimentary basins and orogenic belts and plays an essential role in exploring basin–mountain coupling. It involves determining the palaeoweathering conditions, palaeoclimatic conditions of sedimentary rocks during sedimentary periods, and the geodynamic background of the sedimentary rock's development [1–5]. Methods of provenance tracing include clastic component analysis, heavy mineral analysis, clay mineral analysis, and geochemical element analysis. Due to their homogeneity and low permeability, argillaceous sedimentary rocks (like black shales) retain the geochemical signature of the parent rock and thus serve as an ideal medium for provenance analysis. Therefore, the major and trace elements in shale can be used to reflect the characteristics of the parent rock quantitatively, accurately indicating the source area information, and revealing the tectonic setting of the shales [6–8].

In the Upper Yangtze region (southern China), two sets of organic-rich black shales, known as the Wufeng Formation and Longmaxi Formation, were deposited during the Late Ordovician to Early Silurian period. These shales are widely distributed and have a significant thickness, making them a fundamental layer in developing shale gas in China [6–8]. They are considered a rich source of natural gas, which, if successfully extracted, could play a critical role in satisfying China's energy demands. In the past, the Wufeng Formation and the lower Longmaxi Formation were often studied together. However, the frequent geological events at the Ordovician–Silurian boundary, including the impact of the Guangxi movement [9–12], volcanic activities [13–15], and Hirnantian glaciation [16–19], caused differential sedimentation in the Wufeng Formation and lower Longmaxi Formation. As a result, these formations belong to different geological units with unique tectonic cycles. Therefore, it is necessary to study each of these shales separately. This study focused on the lower Longmaxi Formation (Longmaxi-1 Formation) black shales.

The research on the black shales of Longmaxi-1 in the Upper Yangtze region has largely focused on aspects such as organic matter enrichment [20–25], stratigraphic sequence division [26–30], and siliceous rock genesis [2,25,31–33], with limited attention and discussion given to its provenance analysis.

This investigation focused on the black shales of Longmaxi-1 within the core of the well WY1 located in the Upper Yangtze region. Based on the geochemical characteristics of its major and trace elements, the palaeoweathering conditions of the source area during the deposition of the Early Silurian Longmaxi-1 in the area and the provenance and tectonic setting are clarified. This study is of great significance for reconstructing the palaeoclimatic and palaeogeographical conditions of the Upper Yangtze region in the Early Silurian period.

2. Geological Setting

During the Late Ordovician to Early Silurian period, the South China Plate, composed of the Yangtze Block and the Cathaysia Block, was positioned near the palaeoequator and experienced significant tectonic activity on the northwestern margin of Gondwana [34,35] (Figure 1a). The conversion of the Upper Yangtze region from a shallow-water carbonate platform in the Middle Ordovician to a foreland basin in the Early Silurian was influenced by the convergence of the two tectonic blocks and the ongoing intracontinental orogeny [11,12,36,37]. The presence of land masses, uplifts, and underwater plateaus isolated the Upper Yangtze region from the open sea, resulting in a low-energy and oxygen-deficient sedimentary environment. This physical isolation disrupted the exchange of water and nutrients between the sea and land, favouring the preservation of organic matter and leading to the widespread accumulation of organic-rich black shales in the lower Longmaxi Formation. The black shales in Longmaxi-1 serve as a unique and valuable historical record of the geological, environmental, and biotic conditions that existed in the region at the time of its deposition (Figure 1b).

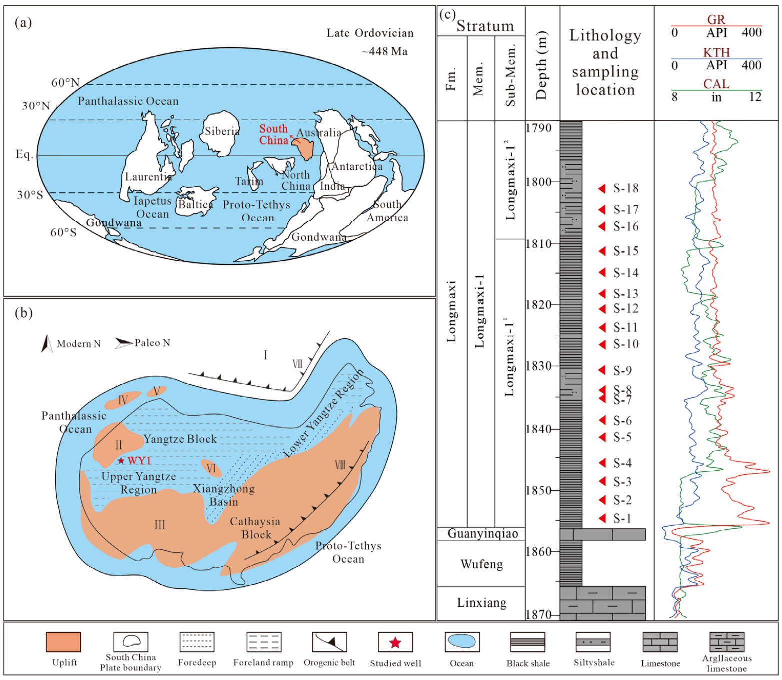

Figure 1. Geological setting of the study sections. (**a**) Late Ordovician global palaeogeographic map [19,38,39]; (**b**) Late Ordovician–Early Silurian Palaeotectonic–Palaeogeographic Map of South

China Plate [40]. Notes: I—North China Plate; II—Chuanzhong Uplift; III—Qianzhong Uplift; IV—Motianling uplift; V—Hannan uplift; VI—Yichang uplift; VII—North Qinling orogenic belt; VIII—Cathaysia orogenic belt. (**c**) Schematic stratigraphic log showing the sample locations.

3. Samples and Methods

3.1. Sample

Eighteen representative samples of Longmaxi-1 were collected from the core of well WY1 located at Neijiang City in Weiyuan County, Sichuan Province, China. As depicted in Figure 1c, the sampling interval averaged approximately 2–4 m. Longmaxi-1 can be divided into Longmaxi-1^1 (samples 1–15) and Longmaxi-1^2 (samples 16–18) in ascending order. The primary lithologies of the specimens include black shales and silty shales, among others. The well-preserved stratigraphic sequence facilitates an accurate representation of the ancient tectonic state.

3.2. Analytical Methods

Selected core samples were meticulously prepared for analysis through rough crushing, rinsing with deionised water, drying, and pulverisation to obtain a fine powder. The powder was then passed through a 200-mesh sieve and stored in polypropylene bags for bulk rock compositional and total organic carbon (TOC) analyses. These analyses were conducted at the Research Institute of Exploration and Development of the PetroChina Southwest Oil & Gasfield Company in Chengdu.

The major element analysis of the samples was conducted utilising X-ray fluorescence spectrometry (XRF, PANalytical Axios mAX, Almelo, Netherlands). Subsequently, the samples were digested with a mixture of HCl, HNO_3, HF, and $HClO_4$, and trace elements were analysed using an inductively coupled plasma mass spectrometer (ICP-MS, PerkinElmer NexION 350X, Waltham, MA, USA). The experimental procedures were in accordance with GB/T 14506-2010.

The total organic carbon (TOC) content of the samples was quantified using a LECO CS-230 carbon–sulphur analyser (LECO Corporation, St. Joseph, MI, USA). Before analysis, a sample aliquot of 100 mg was placed in a crucible with 5% HCl at 80 °C to eliminate any presence of inorganic carbon. The analytical protocol adhered to the guidelines outlined in GB/T 19145-2003.

To ensure the accuracy and precision of the analytical results, a robust quality control protocol was implemented. This included the utilisation of blank samples, replicate analyses, and certified reference materials. The results obtained for all samples were rigorously evaluated against the certified values of the reference materials, with a permissible deviation of ±10%. Additionally, to ensure the reproducibility of the analyses, the relative standard deviation (RSD) of the replicate measurements was stringently constrained to be no more than 5%.

3.3. Data Presentation

3.3.1. Chemical Index of Alteration (CIA)

The chemical Index of Alteration (CIA) is widely used to determine the intensity of palaeoweathering and palaeoclimatic characteristics in the provenance area [41]. If the CIA value is between 85 and 100, it indicates solid chemical weathering, reflecting a hot and humid palaeoclimate; if the CIA value is between 65 and 85, it indicates moderate chemical weathering, reflecting a warm and humid palaeoclimate; if the CIA value is between 50 and 65, it suggests that the provenance area was undergoing initial chemical weathering, reflecting a cold and arid palaeoclimate. The calculation formula for the CIA is as follows:

$$\mathrm{CIA} = [\mathrm{n(Al_2O_3)/(n(Al_2O_3) + n(K_2O) + n(Na_2O) + n(CaO^*))}] \times 100 \tag{1}$$

Furthermore, calculating the weathering index requires the elimination of calcium oxide (CaO) from non-silicate minerals as a preliminary step. This can be achieved by utilising phosphorus pentoxide (P_2O_5) to extract CaO from phosphates, after which the CaO* can be calculated. The calculation formula for the CaO* is as follows:

$$n(CaO_{remaining}) = n(CaO) - n(P_2O_5) \times 10/3 \quad (2)$$

In this formula, if $n(CaO_{remaining}) < n(Na_2O)$, then $(CaO^*) = n(CaO_{remaining})$, whereas if $(CaO_{remaining}) > n(Na_2O)$, then $(CaO^*) = n(Na_2O)$.

3.3.2. Weathering Index of Parker (WIP)

Furthermore, the Weathering Index of Parker (WIP) can distinguish between initial deposition and re-deposition of sediment. However, the usefulness of this index is limited in cases of strong weathering [42,43]. A ratio of CIA/WIP greater than 10 suggests recurrent cycles of sedimentation, while a ratio of CIA/WIP less than 10 indicates primary deposition. The calculation formula for the WIP is as follows:

$$WIP = [2n(Na_2O)/0.35 + n(MgO)/0.9 + 2n(K_2O)/0.25 + n(CaO^*)/0.7] \times 100 \quad (3)$$

3.3.3. Chemical Index of Weathering (CIW)

Additionally, the Chemical Index of Weathering (CIW) can effectively eliminate the interference of K^+ increases due to potassium metasomatism in sediments [44]. The CIW value of Phanerozoic shale is close to 85. If the CIW value > 85, it indicated the chemical solid weathering intensity, and the palaeoclimate in the source area tends to be warm and humid. The calculation formula for the CIW is as follows:

$$CIW = [n(Al_2O_3)/(n(Al_2O_3) + n(N_2O) + n(CaO^*)] \times 100 \quad (4)$$

3.3.4. Index of Compositional Variability (ICV)

The Index of Compositional Variability (ICV) can be employed to evaluate the presence of recycled sediments in the provenance. Shale with low ICV values (less than or equal to 1) is likely derived from a sedimentary source area rich in clay minerals, suggesting that re-deposition or severe weathering occurred after the initial sedimentation, leading to a stronger influence from secondary effects. On the other hand, high ICV values (greater than or equal to 1) indicate that the sediment was initially deposited during a period of tectonic activity [45,46]. The calculation formula for the ICV is as follows:

$$ICV = [n(Fe_2O_3) + n(K_2O) + n(Na_2O) + n(CaO^*) + n(MgO) + n(MnO) + n(TiO_2)]/n(Al_2O_3) \quad (5)$$

4. Results

4.1. Major and Trace Element Contents

The major elements, which include SiO_2, Al_2O_3, CaO, Fe_2O_3, K_2O, and TiO_2, are six of the primary rock-forming elements found in the earth's crust [47]. The content of SiO_2, Al_2O_3, and CaO can generally be correlated to three mineral components: quartz or brittle minerals rich in SiO_2, clay minerals, and carbonates, respectively [36]. These minerals play a significant role in determining the overall composition and properties of rocks. Table 1 shows the major and trace element contents of the Longmaxi-1 black shales in well WY1.

The highest major element in Longmaxi-1^1 black shales was SiO_2 (42.59%–77.53%, avg. = 56.71%), followed by Al_2O_3 (9.31%–18.34%, avg. = 14.06%), and the content of CaO was low (0.97%–16.94%, avg. = 7.62%). In addition, the average contents of Fe_2O_3, K_2O, MgO, Na_2O, TiO_2, P_2O_5, and MnO were 4.41%, 3.42%, 2.98%, 0.80%, 0.57%, 0.15%, and 0.09, respectively. The highest major element in Longmaxi-1^2 black shales was SiO_2 (58.41%–65.78%, avg. = 61.64%), followed by Al_2O_3 (14.08%–17.79%, avg. = 15.52%), with a low content of CaO (0.88%–6.50%, avg. = 3.79%). Additionally, the average contents of

Fe_2O_3, K_2O, MgO, Na_2O, TiO_2, P_2O_5, and MnO were 5.76%, 3.75%, 2.37%, 0.80%, 0.56%, 0.11%, and 0.09%, respectively.

Table 1. Content of major (%) and trace elements (ug/g) in Longmaxi-1 black shales.

Sample	SiO_2	Al_2O_3	Fe_2O_3	MgO	CaO	Na_2O	K_2O	P_2O_5	TiO_2	MnO	Zr	Rb	Th	Sc
S-18	60.73	17.79	6.89	2.75	0.88	0.89	4.25	0.11	0.67	0.06	136.82	180.08	15.16	16.83
S-17	65.78	14.08	5.24	2.13	3.98	0.69	3.41	0.1	0.49	0.09	95.69	137.6	12.92	13.64
S-16	58.41	14.68	5.16	2.24	6.50	0.81	3.59	0.13	0.52	0.12	184.63	142.32	14.73	13.75
S-15	60.36	18.11	6.52	2.84	1.20	0.81	4.43	0.11	0.59	0.06	112.93	187.47	16.69	18.05
S-14	58.98	18.34	6.59	2.94	1.57	0.82	4.46	0.11	0.6	0.06	123.8	188.53	16.84	18.28
S-13	61.01	18.10	6.54	2.83	0.97	0.80	4.47	0.12	0.57	0.05	118.85	182.46	15.31	17.84
S-12	63.59	15.55	4.83	2.51	3.25	0.72	3.92	0.13	0.56	0.05	84.53	156.36	15.78	15.05
S-11	58.01	15.14	5.23	2.64	6.44	0.80	3.69	0.11	0.54	0.09	108.12	149.45	15.96	14.80
S-10	69.49	13.77	5.01	2.20	2.03	0.70	3.40	0.10	0.51	0.05	128.16	134.65	13.71	13.62
S-9	42.59	14.45	3.75	4.70	13.95	0.69	3.51	0.13	0.62	0.15	64.77	113.43	17.07	10.58
S-8	44.34	14.01	3.63	3.03	14.64	0.78	3.31	0.14	0.64	0.1	94.00	106.65	18.76	9.05
S-7	49.66	14.31	4.17	3.18	11.63	0.68	3.49	0.21	0.59	0.10	73.32	121.55	18.56	11.55
S-6	42.66	11.70	4.37	4.64	15.16	0.86	2.58	0.21	0.52	0.16	68.54	81.84	16.02	8.53
S-5	44.13	10.91	3.04	3.53	16.94	0.63	2.71	0.13	0.51	0.15	62.59	89.24	14.91	8.28
S-4	55.11	15.51	4.04	2.80	6.72	1.42	3.58	0.11	0.66	0.05	46.36	79.33	12.94	7.36
S-3	61.83	11.95	3.45	2.65	7.54	1.05	2.73	0.12	0.60	0.08	71.05	93.27	17.95	7.95
S-2	77.53	9.31	2.44	1.65	4.01	0.72	2.36	0.10	0.49	0.04	62.06	84.09	13.75	8.04
S-1	61.40	9.71	2.52	2.63	8.25	0.54	2.63	0.37	0.52	0.15	87.46	91.91	14.85	9.44

Discriminant plates for Zr, Rb, Th, and Sc are often used to discriminate between provenance and tectonic setting [48,49]. The contents of Zr, Rb, Th, and Sc in Longmaxi-1[1] black shales were 46.36–233.88 ug/g (avg. = 95.76 ug/g); 79.33–188.53 ug/g (avg. = 128.90 ug/g); 7.36–18.28 ug/g (avg. = 12.11 ug/g); and 12.92–18.76 ug/g (avg. = 15.69 ug/g), respectively (Table 1).

4.2. Rare Earth Elements

The total rare earth elements content (ΣREE), light rare earth elements (ΣLREE), and heavy rare earth elements (ΣHREE) of Longmaxi-1[1] ranged from 135.68 ug/g to 193.85 ug/g (avg. = 169.08 ug/g); 120.69 ug/g to 176.27 ug/g (avg. = 151.09 ug/g); and 13.5–28.11 ug/g (avg. = 18.00 ug/g), respectively. The ΣREE, ΣLREE, and ΣHREE of Longmaxi-1[2] ranged from 150.32 ug/g to 271.92 ug/g (avg. = 197.18 ug/g); 136.30 ug/g to 245.10 ug/g (avg. = 178.09 ug/g); and 14.02–26.82 ug/g (avg. = 19.09 ug/g), respectively (Table 2).

Table 2. Content of rare earth elements in Longmaxi-1 black shales (ug/g).

Sample	La	Ce	Pr	Nd	Sm	Eu	Gd	Tb	Dy	Ho	Er	Tm	Yb	Lu	ΣLREE	ΣHREE	ΣREE	$(La/Yb)_N$
S-18	40.62	67.33	8.60	29.35	5.52	1.45	4.46	0.85	4.17	0.87	2.47	0.43	2.71	0.46	152.87	16.42	169.29	10.11
S-17	35.12	60.63	7.41	27.47	4.69	0.98	3.97	0.71	3.61	0.72	2.06	0.36	2.23	0.36	136.30	14.02	150.32	10.62
S-16	60.30	106.74	13.67	53.10	9.55	1.74	8.04	1.51	7.13	1.41	3.75	0.64	3.74	0.60	245.10	26.82	271.92	10.87
S-15	45.26	74.76	9.34	33.32	5.88	1.07	4.90	0.91	4.36	0.93	2.28	0.46	2.82	0.43	169.63	17.09	186.72	10.82
S-14	45.04	76.02	9.74	33.63	6.07	1.30	5.00	0.97	4.59	0.95	2.68	0.46	2.93	0.44	171.80	18.02	189.82	10.36
S-13	40.92	69.67	8.55	32.18	5.88	1.12	4.85	0.92	4.42	0.90	2.59	0.45	2.81	0.45	158.32	17.39	175.71	9.82
S-12	38.56	58.18	7.28	26.78	4.29	0.80	3.61	0.69	3.35	0.68	2.00	0.37	2.42	0.38	135.89	13.50	149.39	10.74
S-11	43.44	72.64	9.16	33.90	6.40	1.21	5.44	1.00	4.65	0.94	2.57	0.46	2.81	0.44	166.75	18.31	185.06	10.42
S-10	36.68	62.89	7.74	29.62	5.00	0.98	4.21	0.82	4.00	0.84	2.15	0.42	2.60	0.41	142.91	15.45	158.36	9.51
S-9	31.89	55.79	7.29	28.12	5.27	0.98	4.58	0.86	4.27	0.82	2.27	0.38	2.41	0.37	129.34	15.96	145.30	8.92
S-8	32.41	53.72	6.47	23.30	4.02	0.77	3.56	0.70	3.87	0.83	2.43	0.44	2.74	0.42	120.69	14.99	135.68	7.97
S-7	42.94	65.29	8.49	33.32	6.16	1.07	5.09	0.96	4.52	1.01	2.74	0.49	3.09	0.48	157.27	18.38	175.65	9.37
S-6	32.55	60.94	8.17	34.13	7.48	1.33	6.28	1.17	5.38	1.12	2.88	0.47	2.79	0.42	144.60	20.51	165.11	7.87
S-5	38.28	66.96	8.63	34.40	6.51	1.28	5.72	1.05	4.97	1.03	2.75	0.46	2.82	0.44	156.06	19.24	175.30	9.15
S-4	31.84	58.20	7.19	29.58	6.61	1.18	5.91	1.11	4.96	1.09	2.95	0.49	2.98	0.45	134.60	19.94	154.54	7.20
S-3	42.51	76.93	9.83	38.70	7.04	1.26	5.75	0.93	4.56	0.93	2.08	0.41	2.53	0.39	176.27	17.58	193.85	11.33
S-2	40.10	72.23	9.06	33.96	6.14	0.97	4.55	0.84	3.82	0.80	2.18	0.39	2.49	0.39	162.46	15.46	177.92	10.86
S-1	30.08	53.37	9.01	37.91	7.91	1.46	7.15	1.48	7.38	1.59	4.49	0.75	4.53	0.74	139.74	28.11	167.85	4.48

Notes: $(La/Yb)_N = (La_{sample}/La_{chondritic})/(Yb_{sample}/Yb_{chondritic})$.

The normalised spider diagram of REE was created using the REE content in the Longmaxi-1 black shales. The standardised values used for this graph were obtained from two sources: chondritic meteorites and post-Archaean Australian shale (PAAS). Among them, the normalised spider diagram of chondrite has a clear trend in the text, and PAAS is a commonly used standardized index for sedimentary rocks. The resulting graph (Figure 2) displays the distribution of REEs in the Longmaxi-1 black shales based on these standardised values. The normalised spider diagram of REEs in Longmaxi-1 black shales chondrite showed a steep slope for LREEs and a relatively flat slope for HREEs. Moreover, the normalised spider diagram of the Longmaxi-1 black shales exhibited a variable shape, with dispersed REE content and significant fluctuations, indicating the inhomogeneity and structural instability of the source area.

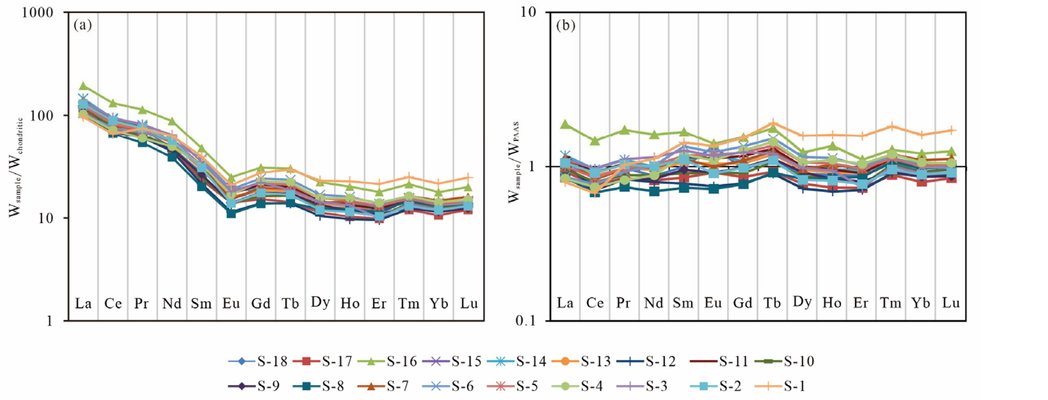

Figure 2. Normalised spider diagram of REEs in Longmaxi-1 black shales. (**a**) Normalised spider diagram of chondritic meteorites; (**b**) normalised spider diagram of PAAS.

4.3. TOC Content

The TOC content of the Longmaxi-1 black shales (Table 3), ranged from 0.75% to 8.21% (avg. = 2.47%). The samples with a TOC content >2% account for 67%, most of which were 2%–3%, and only S-1 was as high as 8%. The TOC content of Longmaxi-1^1 ranged from 0.75% to 8.21% (avg. = 2.62%), with a trend of gradually decreasing TOC content from bottom to top. On the other hand, the TOC content of Longmaxi-1^2 ranged from 0.79% to 2.47% (avg. = 1.69%). These results demonstrate the variability in the TOC content of the different sub-sections of the Longmaxi-1 black shales.

4.4. Palaeoweathering and Palaeoclimate Indices

The palaeoweathering indices of Longmaxi-1 black shales, including CIA, K-correction CIA, WIP, CIW, ICV, SiO_2/Al_2O_3 (SA value), W value, and CIA/WIP were quantified in this study (Table 3). Their respective contents are as follows: 64.47 to 70.91 (avg. = 68.95) for CIA; 68.98 to 82.32 (avg. = 73.70) for K-correction CIA; 32.89 to 55.43 (avg. = 46.66) for WIP; 76.85 to 87.30 (avg. = 84.28) for CIW; 0.89 to 2.51 (avg. = 1.41) for ICV; 2.95 to 8.33 (avg. = 4.20) for the SA value; 44.77 to 78.77 (avg. = 71.09) for W; and 1.18 to 1.99 (avg. = 1.50) for CIA/WIP.

Table 3. Palaeoweathering and palaeoclimate indices in Longmaxi-1 black shales.

Sample	TOC	CIA	K-Correction CIA	WIP	CIW	ICV	SA Value	W Value	CIA/WIP
S-18	0.79	70.62	82.31	53.75	86.40	0.92	3.41	76.26	1.31
S-17	1.80	70.26	80.77	42.78	86.12	1.13	4.67	78.51	1.64
S-16	2.47	69.15	78.85	46.00	84.64	1.28	3.98	72.18	1.50
S-15	0.81	70.83	77.69	54.79	87.17	0.91	3.33	78.50	1.29
S-14	0.75	70.91	76.54	55.43	87.18	0.93	3.22	78.24	1.28
S-13	1.00	70.79	76.03	54.98	87.30	0.89	3.37	78.77	1.29

Table 3. *Cont.*

Sample	TOC	CIA	K-Correction CIA	WIP	CIW	ICV	SA Value	W Value	CIA/WIP
S-12	1.85	70.17	75.64	48.51	86.78	1.02	4.09	78.23	1.45
S-11	2.01	69.56	72.69	47.84	85.19	1.28	3.83	73.59	1.45
S-10	2.45	69.71	71.67	43.01	85.67	1.01	5.05	78.07	1.62
S-9	2.91	70.42	70.77	50.72	86.42	1.88	2.95	73.37	1.39
S-8	2.51	69.50	70.26	45.45	84.52	1.86	3.16	68.63	1.53
S-7	2.43	70.41	69.87	46.24	86.48	1.66	3.47	76.44	1.52
S-6	3.63	67.54	69.49	44.61	80.53	2.40	3.65	58.84	1.51
S-5	2.87	68.55	68.98	40.01	84.03	2.51	4.04	70.21	1.71
S-4	2.40	64.47	70.00	54.49	76.85	1.24	3.55	44.77	1.18
S-3	2.50	65.09	76.03	42.59	77.57	1.51	5.17	54.23	1.53
S-2	3.03	65.41	69.62	32.89	79.72	1.25	8.33	64.08	1.99
S-1	8.21	67.74	69.36	35.81	84.53	1.76	6.32	76.64	1.89

5. Discussion

5.1. Reliability of Chemical Weathering Indices

The extent of palaeoweathering in the provenance of rock can significantly impact the chemical composition of clastic sediments. The palaeoweathering process can cause alkali metal and alkaline earth metal elements such as calcium, potassium, and sodium to move with surface fluids, whereas some stable elements like aluminium and titanium are not affected by weathering and are retained within the sediments [49–52]. Therefore, the presence and relative proportion of specific indices (such as CIA, WIP, PIA, etc.) can serve as an indicator of the extent of chemical weathering in provenance [3,53–55]. Under normal circumstances, the provenance of sediments is complex. When analysing the tectonic setting and provenance characteristics of sedimentary rocks using geochemical element characteristics, the impact of potassium exchange during sedimentary diagenesis, sedimentary recycling, and provenance palaeoweathering should be taken into account first [56,57].

5.1.1. Potassium Metasomatism during Diagenesis

In the Al_2O_3-CaO^*-K_2O (A-CN-K) diagram (Figure 3a), most sample points are distributed along the A-CN direction. Still, there is a certain angle between the actual and ideal weathering lines, indicating that the samples were affected by instances of potassium metasomatism during the deposition period. The CIA value connecting the CN endpoint with the corresponding projection point of the sample on the ideal weathering line is the corrected CIA value excluding potassium metasomatism [41,49,57]. It can be seen that potassium metasomatism reduced the CIA value. Still, the original CIA value and K-correction CIA values all indicated that Longmaxi-1 had experienced a moderate-intensity chemical weathering, indicating that potassium metasomatism had no significant effect on the geochemical characteristics of elements and can be used for provenance analysis (Figure 3a,b).

The CIA value of Longmaxi-1 black shales was in line with the vertical trend of the CIW value, and the two showed a strong positive correlation ($R^2 > 0.9$), as shown in Figure 3c. This supports the conclusion that potassium metasomatism had a limited impact on the CIA value of Longmaxi-1 black shales (Figure 3c).

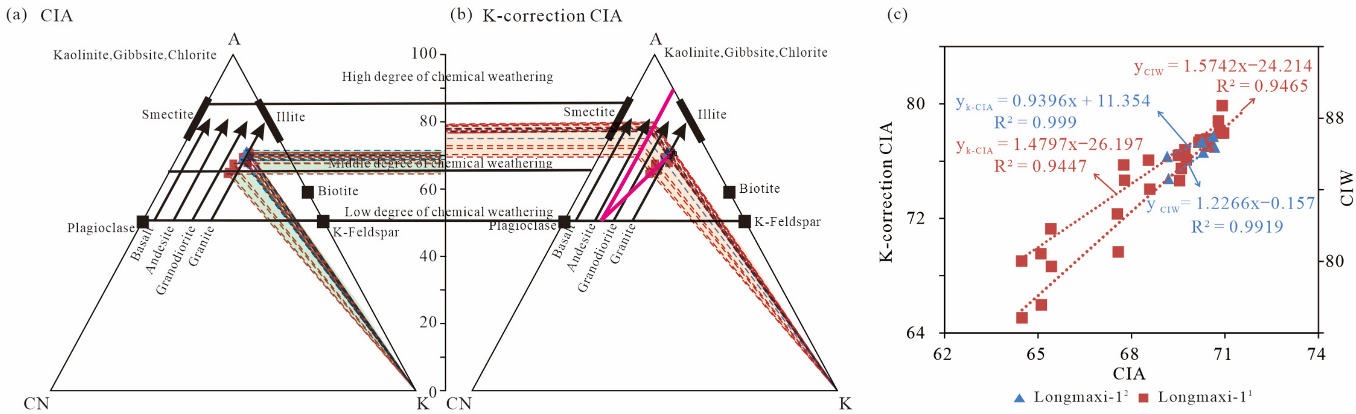

Figure 3. The discrimination diagram of potassium metasomatism in black shales of Longmaxi-1 during diagenesis. (**a**) A-CN-K with uncorrected data [41]; (**b**) A-CN-K with K-corrected data [49]; (**c**) CIA-(K-correction CIA)/CIW [41,49,57].

5.1.2. Maturity of Sediment Composition and Sedimentary Recycling

The maturity of sediment composition is associated with its depositional environment and tectonic setting. Indicators such as the silicon–aluminium ratio (SA value), ICV value, WIP indices, and MFW triangle diagram of clastic sediments can all reveal the maturity of sediment composition and sedimentary recycling [42,43,45,46,58,59]. It is a widely held belief that an average value of SA greater than 5 signifies a high degree of compositional maturity in sediments, while a value less than 5 suggests immaturity [45]. The Longmaxi-1 black shales displayed SA values ranging from 2.95 to 8.33 (avg. = 4.20), ICV values ranging from 0.87 to 2.51 (avg. = 1.41), and CIA/WIP values ranging from 0.80 to 0.84 (avg. = 0.82), suggesting that the maturity of the sediment composition of the shales was low and resulted from primary sedimentation (Figure 4). As illustrated in Figure 5, the sample sites are predominantly situated in semi-arid regions and regions of low maturity, indicating that the Longmaxi-1 black shales are products of initial sedimentation and have not undergone the impact of recycled processes. The MFW triangular diagram can aid in differentiating the types of cyclic sedimentation and reflect the composition of the initial parent rock of the sediment [58]. The trend line of the shale composition in Figure 6 intersects with the trend line of igneous rocks, suggesting that the Longmaxi-1 black shales originate from igneous rocks and possess features associated with primary deposition.

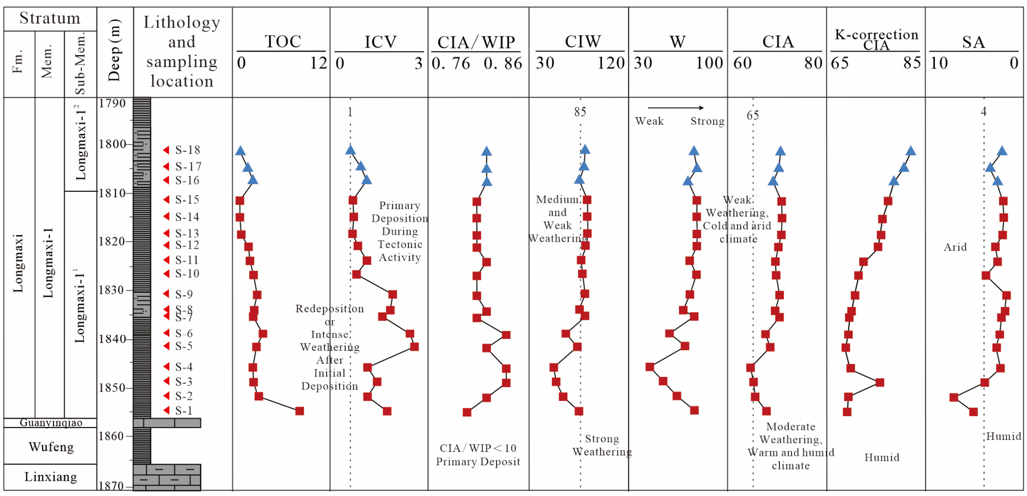

Figure 4. The vertical variation of TOC content and weathering indices in Longmaxi-1 black shales.

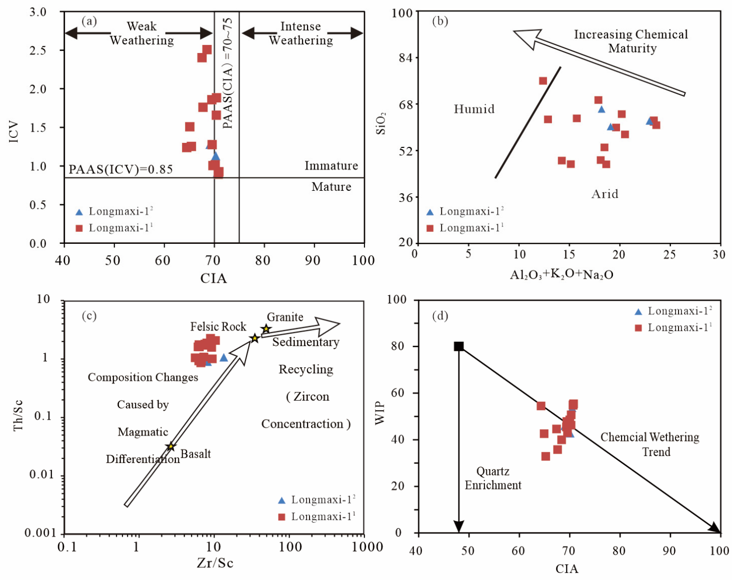

Figure 5. The discrimination diagram of palaeoweathering intensity and maturity in Longmaxi-1 black shales. (**a**) CIA-ICV [45]; (**b**) (Al_2O_3+K_2O+Na_2O)-SiO_2 [60]; (**c**) Zr/Sc-Th/Sc [48]; (**d**) CIA-WIP [43].

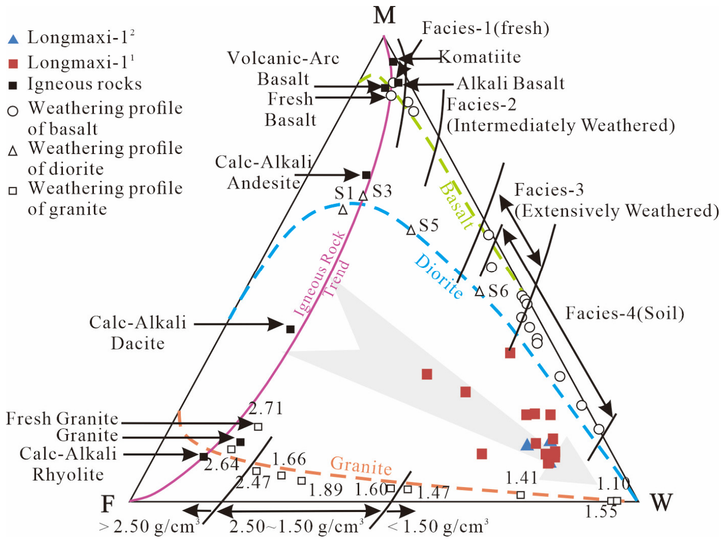

Figure 6. WFM discriminant diagram in Longmaxi-1 black shales [58]. M, F, and W represent the mafic source, felsic source, and weathered material, respectively. The broken lines are linear compositional trends for igneous, diorite, and granite weathering profiles.

5.2. Palaeoweathering and Palaeoclimate

A complex interplay of factors, including palaeoclimate conditions and tectonic activity, shapes the palaeoweathering process. In particular, when the climate was characterised by extreme cold and arid conditions, it resulted in a weakened chemical weathering intensity. To properly assess the extent of weathering that occurred during the formation of shales, it is necessary to consider a combination of geochemical indicators. This multidisciplinary approach provides a more comprehensive picture of the weathering process and its impact on rock formation.

The vertical profiles of the CIA, CIW, and W values depicted in Figure 4 exhibited similar variations. During the Longmaxi-1[1] shales sedimentation period, the shales experienced a gradual decrease in palaeoweathering intensity at a depth of 1853.76–1844.89 m, which reached its maximum at 1840.70 m. Between 1840.70 and 1823.11 m, the shales displayed a pattern of two consecutive declines in palaeoweathering intensity followed by an increase, whereas, between 1829.96 and 1810.84 m, the shales demonstrated a stable trend in palaeoweathering intensity. During the Longmaxi-1^2 shale sedimentation period, the shales reached the highest level of palaeoweathering intensity at 1860.70 m but then decreased. The vertical variations of CIA and K-correction CIA are illustrated in Figure 4, revealing that Longmaxi-1 was predominantly deposited in humid climatic conditions. Based on the analysis above, the Longmaxi-1 black shales appear to exhibit vertical instability despite being deposited in a generally humid climate. This phenomenon may be attributed to the Late Ordovician Hirnantian glaciation, which caused fluctuations in the climatic conditions during the Early Silurian [61–63].

In addition, the SA value can also indicate palaeoclimatic conditions. When the SA value exceeds 4, it signifies a dry climate with predominating physical weathering, while an SA value of less than 4 indicates a humid environment where chemical weathering is prevalent [59]. The average SA value of the Longmaxi-1 black shales was 4.20, but vertically, the SA value mainly indicated a humid environment (Figure 4).

5.3. Provenance

The geochemical characteristics of sedimentary rocks are related to their source area and tectonic setting during formation. The provenance properties are essential in affecting the sedimentary rocks' chemical composition [64–66]. Section 4.2 engaged in a detailed analysis of the rare earth element characteristics of the black shales found in Longmaxi-1 within the scope of this study. The analysis results indicated that the black shales contained acidic substances in the parent rock. Furthermore, the Rb-K_2O, A-CNK-FM, and REE-La/Yb provenance intersection diagrams and the $F_2{}^1$-$F_1{}^1$ discrimination function diagram also demonstrated that the black shales in Longmaxi-1 were sourced from a diverse region, primarily composed of intermediate-acid granite and granodiorite (Figure 7a,b), with some contribution from basalt (the middle part of Figure 7c) and quartzite (the lower left of Figure 7d). These findings are similar to those of previous studies showing that the parent rock of Longmaxi-1 in the Upper Yangtze region was mainly acidic igneous rock [67–71]. Moreover, the mapping results of quartzite and basalt as parent rock may indicate more than two mixture provenances in the Upper Yangtze region during this period.

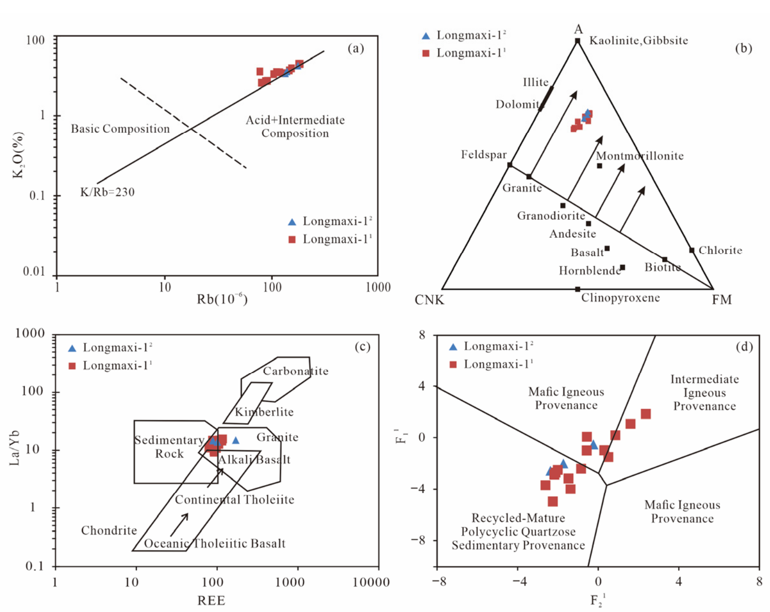

Figure 7. Provenance discrimination diagram in Longmaxi-1 black shales. (**a**) Rb-K_2O [72]; (**b**) A-CNK-FM [73]; (**c**) REE-La/Yb [74]; (**d**) $F_2{}^1$-$F_1{}^1$ discrimination function diagram [75].

5.4. Geodynamic Background of Black Shales Development

At present, the orogenic model of the Early Palaeozoic South China Plate is still controversial. The focus is on whether the dynamic mechanism of the Yangtze–Cathaysia Block is subduction collision orogeny or intracontinental orogeny. In other words, whether there is an unknown subduction of oceanic crust at the southern margin of the South China Plate is unclear [76–80]. However, in recent years, numerous studies have shown that no contemporaneous volcanic rocks, island arc magmatic rocks, and deep-sea or oceanic-related sedimentary rocks such as ophiolite complex and turbidite rocks were found in the South China Plate during the Early Palaeozoic. The South China Block should be considered a continuous and unified continental landmass, with the amalgamation of the Yangtze–Cathaysia Block primarily driven by intracontinental orogeny [9,10,81]. The tectonic driving factors are related to subduction collision between the South China and North China Plates or the remote interaction between the South China Block and the East Gondwana Plate's northern margin [12,77,82–84]. We agree that the tectonic attribute of the South China Block in the Early Palaeozoic is intracontinental orogeny. On this basis, the provenance analysis of the Longmaxi-1 black shales in the Upper Yangtze region was carried out.

Shale composition is closely associated with its formation period and tectonic setting, exhibiting specific geochemical characteristics in different tectonic environments [64,65,72,74,85–87]. The tectonic setting of Longmaxi-1 black shales in the Upper Yangtze region was studied based on its major and trace element composition. Using ternary diagrams and the discriminant function diagram proposed by Verma, we have partially identified island arc volcanic characteristics in some of the Longmaxi-1 black shales, as shown in Figure 8a–c. This observation is likely related to the subduction of the North Qinling Ocean [83–86].

Verma and Armstrong have created discriminant function diagrams (DF1-DF2) to effectively distinguish between tectonic settings (island arc, continental rift, and subduction collision orogeny) of high-silica [$(SiO_2)_{adj}$ = 63%–95%] and low-silica [$(SiO_2)_{adj}$ = 35%–63%] clastic sediments, overcoming the limitations of traditional diagrams in normalising sample compositional data [88]. Of the analysed samples, 14 had a SiO_2 content > 63% and belonged to high-silica shales, while 4 were low-silica shales. The projection points of the samples in Figure 8d,e were all located within a subduction collision orogeny sedimentary environment, indicating that the sedimentary tectonic setting of Longmaxi-1 was dominated by collisional orogeny. In summary, based on the concentration, proportion, and normalised REE patterns of major and trace elements, we suggest that an active continental margin and island arc-continent collision characterise the tectonic environment of the Longmaxi-1 black shales.

5.5. Comparative Analysis of Provenance

The tectonic setting and provenance of the Early Silurian South China Block remain a matter of ongoing debate and have yet to reach a consensus. Zhang reported that the ancient Kangding–Yunnan Land blanket provides the primary provenance of the Longmaxi black shales in Southwest Sichuan during the Early Neoproterozoic [89]. Liu and Xiong contend that the Hannan uplift and Bashan uplift on the northern margin of the Yangtze Block provided material provenance for the basin [90,91]. Li suggested that there may have been a mixed provenance in the Longmaxi Formation in northern Guizhou [92]. By using the well WY1 and previously published cores from the same time period that are representative of the region, the provenance can be directly shown based on the REE normalised spider diagram and $(La/Yb)_N$ variation.

The REE normalised spider diagram of Longmaxi-1 black shales in the well WY1, when compared with those in TBO [90], HD 1 [93], TLO [94], STO [95], and QQ1 [96], were found to be similar to the patterns shown in Figure 9. These patterns exhibited an apparent negative Eu anomaly with a right-leaning "V" shape, while STP showed a positive Eu anomaly (Figure 9). This suggests that the main provenance of Longmaxi-1 is not from the ancient Kangding–Yunnan Land blanket during the Early Neoproterozoic.

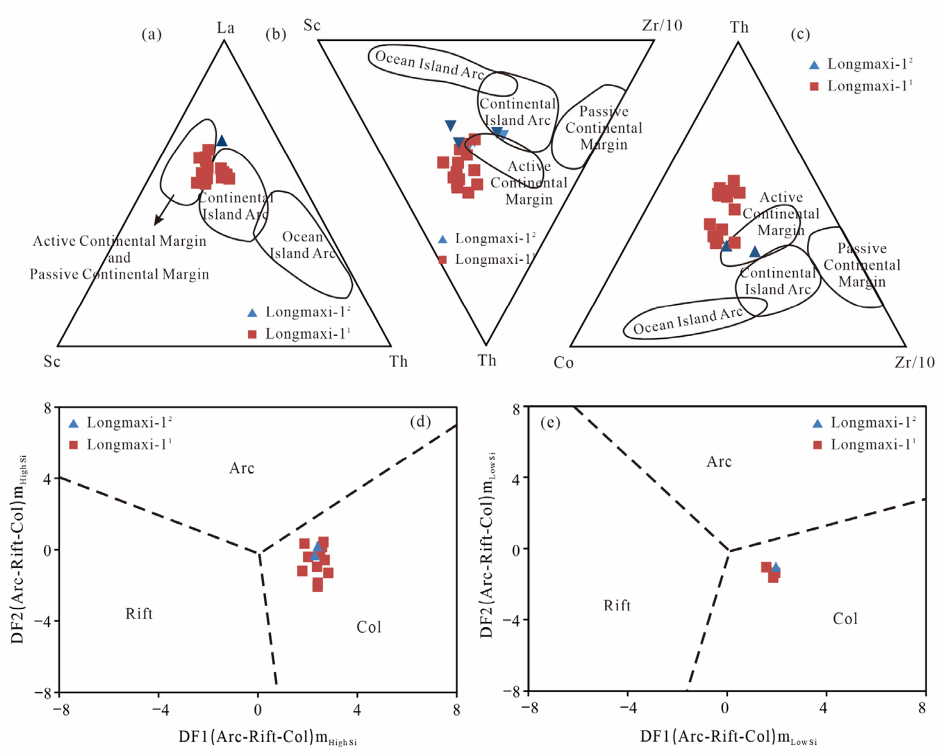

Figure 8. Tectonic setting discrimination diagram in Longmaxi-1 black shales. (**a**–**c**) La-Sc-Th, Th-Zr/10-Sc, Th-Co-Zr/10 [87]; (**d**,**e**) DF1-DF2 discrimination function diagrams [89]. Notes: Arc—land arc; Rift—continental rift; Col—subduction collision orogeny.

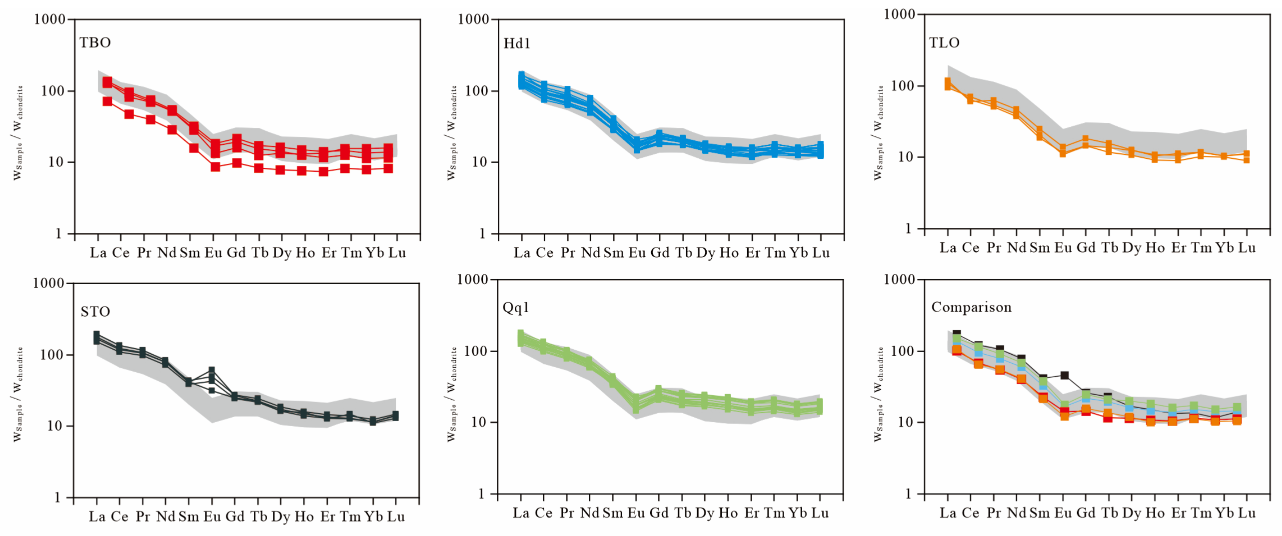

Figure 9. REE normalised spider diagram of Longmaxi-1 black shales in different provenances. Notes: TBO—Tianba Outcrop; HD1—Well of Huadi 1; TLO—Tianlin Outcrop; STO—Sutian Outcrop; QQ1—Well of Qianqian 1; the shaded area represents normalised spider diagram of REEs in Longmaxi-1 black shales of well WY1.

The $(La/Yb)_N$ value reflects the degree of fractionation of LREEs and HREEs, with lower $(La/Yb)_N$ values indicating a greater distance from the provenance and higher $(La/Yb)_N$ values indicating closer proximity [97]. The Longmaxi-1 sedimentary period showed high $(La/Yb)_N$ values northeast of the Yangtze Block (Figure 10), suggesting proximity to the provenance and the North Qiangling Orogenic Belt may have provided the provenance. The high value of $(La/Yb)_N$ in the QQ1 area is different from that in the HD1 area, indicating that there is another high-value area in the southeast direction, indicating that the Cathaysia Orogenic Belt continued to shorten and experience tectonic loading in the Silurian, and provided a particular provenance [98]. Therefore, we speculate that the Cathaysian orogenic belt and the North Qiangling orogenic belt may contribute to the formation of Longmaxi-1 black shales in the Upper Yangtze region.

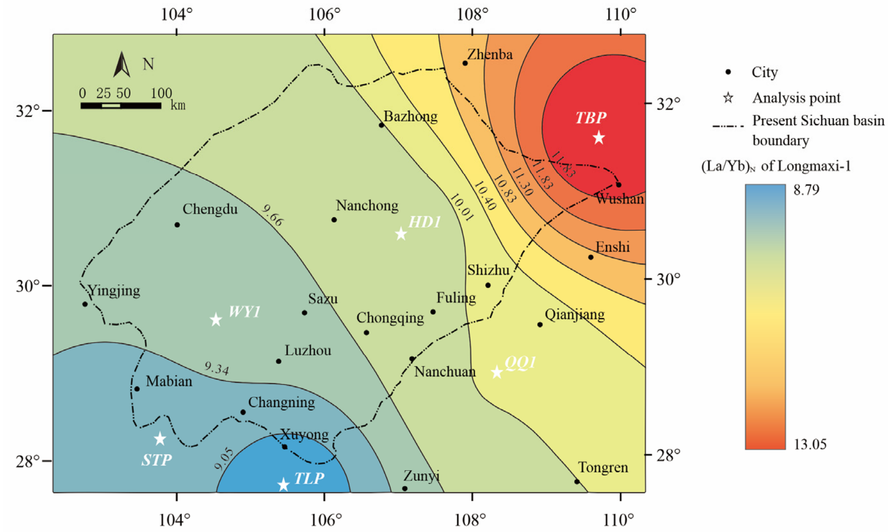

Figure 10. The distribution of $(La/Yb)_N$ of the Upper Yangtze region (southern China) during the sedimentary period of Longmaxi-1 in Early Silurian.

6. Conclusions

By studying the geochemical characteristics of the black shales of Longmaxi-1 in the Upper Yangtze region and taking into consideration the palaeoweathering conditions in the source area and the tectonic conditions of the Upper Yangtze region (southern China), the following conclusions have been reached:

The weathering indicators such as CIA, CIV, WIP, CIW, and the ratio of SiO_2/Al_2O_3 showed that the Longmaxi-1 black shales were the first deposit during the period of tectonic activity, with an immature composition and structure. The palaeoclimate of the source area was warm and humid as a whole, but it fluctuated in vertical change.

The Rb-K_2O, A-CNK-FM, and REE-La/Yb provenance intersection diagrams and F_2^1-F_1^1 discrimination function diagram collectively suggested that the parent rock for the black shales in Longmaxi-1 are were intermediate-acidic granites and granodiorites. In addition, there were also recycled-mature quartzose and basaltic provenances present. La-Sc-Th, Th-Zr/10-Sc, and Th-Co-Zr/10 tectonic setting discriminant diagrams and DF1-DF2 discriminant function diagrams showed that the tectonic setting of the provenance was mainly the active continental margin and island arc-continent collision. Drawing on the findings of provenance analysis and tectonic setting investigation, we can plausibly posit that the Cathaysian orogenic belt and the North Qiangling orogenic belt may have played a role in the genesis of the Longmaxi-1 black shales within the Upper Yangtze region.

Author Contributions: Conceptualization, Y.L.; methodology, L.Z.; software, C.W.; formal analysis, C.Z.; writing—original draft preparation, L.Z.; supervision, S.Z.; All authors contributed to the writing of the manuscript. All authors have read and agreed to the published version of the manuscript.

Funding: This research was funded by the Free Inquiry Fund of the State Key Laboratory of Oil and Gas Reservoir Geology and Exploitation (Chengdu University of Technology, China), grant number SKL2019015, and the Science Foundation of the CNPC Chuanqing Drilling Company, grant number CQCDLG-2020-02.

Data Availability Statement: The data presented in this study are available in the article.

Acknowledgments: We acknowledge the constructive reviews from three anonymous reviewers and editorial assistant editor.

Conflicts of Interest: The authors declare no conflict of interest.

References

1. Ge, X.; Mou, C.; Yu, Q.; Liu, W.; Men, X.; He, J. The geochemistry of the sedimentary rocks from the Huadi No. 1 well in the Wufeng-Longmaxi formations (Upper Ordovician-Lower Silurian), South China, with implications for paleoweathering, provenance, tectonic setting and paleoclimate. *Mar. Pet. Geol.* **2019**, *103*, 646–660. [CrossRef]
2. Abubakar, U.; Usman, M.B.; Aliyuda, K.; Dalha, A.; Bello, A.M.; Linus, L.N. Major and trace element geochemistry of the shales of Sekuliye Formation, Yola Sub-Basin, Northern Benue Trough, Nigeria: Implications for provenance, weathering intensity, and tectonic setting. *J. Sediment. Environ.* **2021**, *6*, 473–484. [CrossRef]
3. Chen, L.; Zhang, B.; Jiang, S.; Chen, X.; Zhang, G.; Zhang, J.; Wei, W.; Lu, Y.; Chen, P.; Lin, W.; et al. Provenance, source weathering, and tectonic setting of the lower Cambrian Shuijingtuo Formation in the Middle Yangtze area, China. *Mar. Pet. Geol.* **2022**, *139*, 105584. [CrossRef]
4. Ofili, S.; Soesoo, A.; Panova, E.G.; Hints, R.; Hade, S.; Ainsaar, L. Geochemical Reconstruction of the Provenance, Tectonic Setting and Paleoweathering of Lower Paleozoic Black Shales from Northern Europe. *Minerals* **2022**, *12*, 602. [CrossRef]
5. Li, J.; Tian, J.; Zhang, X.; Liang, Q.; Peng, M. Geochemical characteristics and the constraints on paleoenvironment, provenance, and tectonic setting of Precambrian Xifangshan Formation in the northwestern Tarim Basin, NW China. *J. Pet. Sci. Eng.* **2022**, *208*, 109553. [CrossRef]
6. Zou, C.; Zhu, R.; Chen, Z.; Ogg, J.G.; Wu, S.; Dong, D.; Qiu, Z.; Wang, Y.; Wang, L.; Lin, S.; et al. Organic-matter-rich shales of China. *Earth-Sci. Rev.* **2019**, *189*, 51–78. [CrossRef]
7. Guo, X.; Hu, D.; Huang, R.; Wei, Z.; Duan, J.; Wei, X.; Fan, X.; Miao, Z. Deep and ultra-deep natural gas exploration in the Sichuan Basin: Progress and prospect. *Nat. Gas Ind. B* **2020**, *7*, 419–432. [CrossRef]
8. Yan, D.; Li, S.; Fu, H.; Jasper, D.M.; Zhou, S.; Yang, X.; Zhang, B.; Mangi, H.N. Mineralogy and geochemistry of Lower Silurian black shales from the Yangtze platform, South China. *Int. J. Coal Geol.* **2021**, *237*, 103706. [CrossRef]
9. Chen, X.; Zhang, Y.; Fan, J.; Tang, L.; Sun, H. Onset of the Kwangsian Orogeny as evidenced by biofacies and lithofacies. *Sci. China Earth Sci.* **2012**, *42*, 1617–1626. [CrossRef]
10. Chen, X.; Fan, J.; Chen, Q.; Tang, L.; Hou, X. Toward a stepwise Kwangsian Orogeny. Science China. *Sci. China Earth Sci.* **2014**, *44*, 842–850. [CrossRef]
11. Xu, Y.; Cawood, P.; Du, Y. Intraplate orogenesis in response to Gondwana assembly: Kwangsian Orogeny, South China. *Am. J. Sci.* **2016**, *316*, 329–362. [CrossRef]
12. Shu, L.; Yao, J.; Wang, B.; Faure, M.; Charvet, J.; Chen, Y. Neoproterozoic plate tectonic process and Phanerozoic geodynamic evolution of the South China Block. *Earth-Sci. Rev.* **2021**, *216*, 103596. [CrossRef]
13. Shen, J.; Wang, P.; Chen, K.; Zhang, D.; Wang, Y.; Cai, Q.; Meng, J. Relationship between volcanic activity and enrichment of shale organic matter during the Ordovician-Silurian transition in western Hubei, Southern China. *Palaeogeogr. Palaeoclimatol. Palaeoecol.* **2021**, *577*, 110551. [CrossRef]
14. Wu, L.; Lu, Y.; Jiang, S.; Liu, X.; Liu, Z.; Lu, Y. Relationship between the origin of organic-rich shale and geological events of the Upper Ordovician-Lower Silurian in the Upper Yangtze area. *Mar. Pet. Geol.* **2019**, *102*, 74–85. [CrossRef]
15. Yang, X.; Yan, D.; Zhang, B.; Zhang, L.; Wei, X.; Li, T.; Zhang, J.; She, X. The impact of volcanic activity on the deposition of organic-rich shales: Evidence from carbon isotope and geochemical compositions. *Mar. Pet. Geol.* **2021**, *128*, 105010. [CrossRef]
16. Delabroye, A.; Vecoli, M. The end-Ordovician glaciation and the Hirnantian Stage: A global review and questions about Late Ordovician event stratigraphy. *Earth-Sci. Rev.* **2010**, *98*, 269–282. [CrossRef]
17. Rong, J.; Chen, X.; Wang, Y.; Zhan, R.; Liu, J.; Huang, B.; Tang, P.; Wu, R.; Wang, G. Northward expansion of Central Guizhou Oldland through the Ordovician and Silurian transition: Evidence and implications. *Sci. China Earth Sci.* **2011**, *41*, 1407–1415. [CrossRef]
18. Li, N.; Li, C.; Algeo, T.J.; Cheng, M.; Jin, C.; Zhu, G.; Fan, J.; Sun, Z. Redox changes in the outer Yangtze Sea (South China) through the Hirnantian Glaciation and their implications for the end-Ordovician biocrisis. *Earth-Sci. Rev.* **2021**, *212*, 103443. [CrossRef]
19. Lu, Y.; Huang, C.; Jiang, S.; Zhang, J.; Lu, Y.; Liu, Y. Cyclic late Katian through Hirnantian glacioeustasy and its control of the development of the organic-rich Wufeng and Longmaxi shales, South China. *Palaeogeogr. Palaeoclimatol. Palaeoecol.* **2019**, *526*, 96–109. [CrossRef]
20. Wang, Y.; Li, X.; Dong, D.; Zhang, C.; Wang, S. Major controlling factors for the high-quality shale of Wufeng–Longmaxi Formation, Sichuan Basin. *Energy Explor. Exploit.* **2017**, *35*, 444–462. [CrossRef]
21. Li, Y.; Zhang, T.; Ellis, G.S.; Shao, D. Depositional environment and organic matter accumulation of Upper Ordovician–Lower Silurian marine shale in the Upper Yangtze Platform, South China. *Palaeogeogr. Palaeoclimatol. Palaeoecol.* **2017**, *466*, 252–264. [CrossRef]
22. Yan, D.; Chen, D.; Wang, Z.; Li, J.; Yang, X.; Zhang, B. Climatic and oceanic controlled deposition of Late Ordovician-Early Silurian black shales on the North Yangtze platform, South China. *Mar. Pet. Geol.* **2019**, *110*, 112–121. [CrossRef]

23. Qiu, Z.; Zou, C. Controlling factors on the formation and distribution of "sweet-spot areas" of marine gas shales in South China and a preliminary discussion on unconventional petroleum sedimentology. *J. Asian Earth Sci.* **2020**, *194*, 103989. [CrossRef]
24. Chen, L.; Jiang, S.; Chen, P.; Chen, X.; Zhang, B.; Zhang, G.; Lin, W.; Lu, Y. Relative sea-level changes and organic matter enrichment in the Upper Ordovician-Lower Silurian Wufeng-Longmaxi Formations in the Central Yangtze area, China. *Mar. Pet. Geol.* **2021**, *124*, 104809. [CrossRef]
25. Cai, Q.; Hu, M.; Kane, O.I.; Li, M.; Zhang, B.; Hu, Z.; Deng, Q.; Xing, N. Cyclic variations in paleoenvironment and organic matter accumulation of the Upper Ordovician–Lower Silurian black shale in the Middle Yangtze Region, South China: Implications for tectonic setting, paleoclimate, and sea-level change. *Mar. Pet. Geol.* **2022**, *136*, 105477. [CrossRef]
26. Chen, L.; Lu, Y.; Jiang, S.; Li, J.; Guo, T.; Luo, C. Heterogeneity of the Lower Silurian Longmaxi marine shale in the southeast Sichuan Basin of China. *Mar. Pet. Geol.* **2015**, *65*, 232–246. [CrossRef]
27. Guo, X. Sequence Stratigraphy and Evolution Model of the Wufeng-Longmaxi Shale in the Upper Yangtze Area. *Earth Sci.* **2017**, *42*, 1069–1082. [CrossRef]
28. Chen, X.; Fan, J.; Wang, W.; Wang, H.; Nie, H.; Shi, X.; Wen, Z.; Chen, D.; Li, W. Stage-progressive distribution pattern of the Lungmachi black graptolitic shales from Guizhou to Chongqing, Central China. *Sci. China Earth Sci.* **2017**, *47*, 720–732. [CrossRef]
29. Wang, G.; Jin, Z.; Hu, Z.; Liu, G.; Zhu, T.; Du, W.; Wang, H.; Wu, J. Sedimentary Evolution Characteristics of Fine-Grained Lithofacies under the High-Resolution Isochronous Shelf System: Insights from the Wufeng-Longmaxi Shales in the Sichuan Basin. *Lithosphere* **2021**, *2021*, 6628867. [CrossRef]
30. Zhao, S.; Li, Y.; Xu, Y.; Cheng, L.; Nie, Z.; Zhao, L. Earth's Orbital Control on Organic Matter Enrichment in the Black Shales of the Wufeng–Longmaxi Formation in the Upper Yangtze Region, South China. *Front. Earth Sci.* **2022**, *10*, 938323. [CrossRef]
31. Guan, Q.; Dong, D.; Zhang, H.; Sun, S.; Zhang, S.; Guo, W. Types of biogenic quartz and its coupling storage mechanism in organic-rich shales: A case study of the Upper Ordovician Wufeng Formation to Lower Silurian Longmaxi Formation in the Sichuan Basin, SW China. *Pet. Explor. Dev.* **2021**, *48*, 813–823. [CrossRef]
32. Xu, H.; Zhou, W.; Hu, Q.; Yi, T.; Ke, J.; Zhao, A.; Lei, Z.; Yu, Y. Quartz types, silica sources and their implications for porosity evolution and rock mechanics in the Paleozoic Longmaxi Formation shale, Sichuan Basin. *Mar. Pet. Geol.* **2021**, *128*, 105036. [CrossRef]
33. Ye, Y.; Tang, S.; Xi, Z.; Jiang, D.; Duan, Y. Quartz types in the Wufeng-Longmaxi Formations in southern China: Implications for porosity evolution and shale brittleness. *Mar. Pet. Geol.* **2022**, *137*, 105479. [CrossRef]
34. Zou, C.; Qiu, Z.; Poulton, S.W.; Dong, D.; Wang, H.; Chen, D.; Lu, B.; Shi, Z.; Tao, H. Ocean euxinia and climate change "double whammy" drove the Late Ordovician mass extinction. *Geology* **2018**, *46*, 535–538. [CrossRef]
35. Torsvik, T.; Cocks, L. Gondwana from top to base in space and time. *Gondwana Res.* **2013**, *24*, 999–1030. [CrossRef]
36. Chen, X.; Rong, j.; Li, Y.; Boucot, A.J. Facies patterns and geography of the Yangtze region, South China, through the Ordovician and Silurian transition. *Palaeogeogr. Palaeoclimatol. Palaeoecol.* **2004**, *204*, 353–372. [CrossRef]
37. Zhou, K.; Mou, C.; Xu, X.; Ge, X.; Liang, W. Early Silurian paleogeography and source-reservoir-cap rocks of the Middle-Upper Yangtze region in South China. *Pet. Explor. Dev.* **2014**, *41*, 684–694. [CrossRef]
38. Metcalfe, I. Late Palaeozoic and Mesozoic Palaeogeography of Eastern Pangea and Tethys. *Pangea Glob. Environ. Resour.* **1994**, *17*, 97–111.
39. Egozcue, J.J.; Pawlowsky-Glahn, V.; Mateu-Figueras, G.; Barceló-Vidal, C. Isometric Logratio Transformations for Compositional Data Analysis. *Math. Geol.* **2003**, *35*, 279–300. [CrossRef]
40. Huang, H.; He, D.; Li, D.; Li, Y.; Zhang, W.; Chen, J. Geochemical characteristics of organic-rich shale, Upper Yangtze Basin: Implications for the Late Ordovician–Early Silurian orogeny in South China. *Palaeogeogr. Palaeoclimatol. Palaeoecol.* **2020**, *554*, 109822. [CrossRef]
41. Nesbitt, H.; Young, G. Prediction of some weathering trends of plutonic and volcanic rocks based on thermodynamic and kinetic considerations. *Geochim. Cosmochim. Acta* **1984**, *48*, 1523–1534. [CrossRef]
42. Parker, A. An Index of Weathering for Silicate Rocks. *Geol. Mag.* **1970**, *107*, 501–504. [CrossRef]
43. Garzanti, E.; Padoan, M.; Andò, S.; Resentini, A.; Vezzoli, G.; Lustrino, M. Weathering and Relative Durability of Detrital Minerals in Equatorial Climate: Sand Petrology and Geochemistry in the East African Rift. *J. Geol.* **2013**, *121*, 547–580. [CrossRef]
44. Harnois, L. The CIW index: A new chemical index of weathering. *Sediment. Geol.* **1988**, *55*, 319–322. [CrossRef]
45. Cox, R.; Lowe, D.R.; Cullers, R.L. The influence of sediment recycling and basement composition on evolution of mudrock chemistry in the southwestern United States. *Geochim. Cosmochim. Acta* **1995**, *59*, 2919–2940. [CrossRef]
46. Van De Kamp, P.C.; Leake, B.E. Petrography and geochemistry of feldspathic and mafic sediments of the northeastern Pacific margin. *Trans. R. Soc. Edinb. Earth Sci.* **1985**, *76*, 411–449. [CrossRef]
47. He, L.; Wang, Y.; Chen, D.; Wang, Q.; Wang, C. Relationship between sedimentary envi ronment and organic matter accumulation in the black shale of Wufeng-Longmaxi Formations in Nanchuan area, Chongqing. *Nat. Gas Geosci.* **2019**, *30*, 203–218.
48. McLennan, S.M.; Hemming, S.; McDaniel, D.K.; Hanson, G.N. Geochemical approaches to sedimentation, provenance, and tectonics. *Spec. Pap. Geol. Soc. Am.* **1993**, 21.
49. Fedo, C.M.; Wayne Nesbitt, H.; Young, G.M. Unraveling the effects of potassium metasomatism in sedimentary rocks and paleosols, with implications for paleoweathering conditions and provenance. *Geology* **1995**, *23*, 921. [CrossRef]
50. Nesbitt, H.W.; Young, G.M. Early Proterozoic climates and plate motions inferred from major element chemistry of lutites. *Nature* **1982**, *299*, 715–717. [CrossRef]

51. Cai, G.; Guo, F.; Liu, X.; Sui, S. Clastic Aediment geochemistry: Implication for Provenance and Tectonic Setting and Its Influential Factors. *Earth Environ.* **2006**, 75–83.
52. Wang, Z.; Zhan, W.; Gao, Y.; Xiao, Y. Provenance and tectonic setting analysis of the Upper Triassic Zangxiahe Formation sandstone in the Northern Qiangtang Basin. *Geol. Rev.* **2020**, *66*, 1199–1216.
53. Hossain, H.M.Z.; Hossain, Q.H.; Kamei, A.; Araoka, D.; Sultan-Ul-Islam, M. Geochemical characteristics of Gondwana shales from the Barapukuria basin, Bangladesh: Implications for source-area weathering and provenance. *Arab. J. Geosci.* **2020**, *13*, 111. [CrossRef]
54. Masidul Haque, M.; Kanti Roy, M. Sandstone-Shale Geochemistry of Miocene Surma Group in Bandarban Anticline, SE Bangladesh: Implications for Provenance, Weathering, and Tectonic Setting. *Earth Sci.* **2020**, *9*, 38. [CrossRef]
55. Qadrouh, A.N.; Alajmi, M.S.; Alotaibi, A.M.; Baioumy, H.; Almalki, M.A.; Alyousif, M.M.; Ahmed Salim, A.M.; Bin Rogaib, A.M. Mineralogical and geochemical imprints to determine the provenance, depositional environment, and tectonic setting of the Early Silurian source rock of the Qusaiba shale, Saudi Arabia. *Mar. Pet. Geol.* **2021**, *130*, 105131. [CrossRef]
56. Shields, G.; Stille, P. Diagenetic constraints on the use of cerium anomalies as palaeoseawater redox proxies: An isotopic and REE study of Cambrian phosphorites. *Chem. Geol.* **2001**, *175*, 29–48. [CrossRef]
57. Zhang, J.; Mou, C.; Zhou, K.; Feng, L.; Wu, H.; Chen, X. Geochemical Characteristic of Sandstons from the Mangbang Formation in the Husa Basin, Western Yuannan, and Its Constraints on Provenance and Tctonic Setting. *Acta Geol. Sin.* **2017**, *91*, 1083–1096.
58. Ohta, T.; Arai, H. Statistical empirical index of chemical weathering in igneous rocks: A new tool for evaluating the degree of weathering. *Chem. Geol.* **2007**, *240*, 280–297. [CrossRef]
59. Zhang, W.; Mu, K.; Cui, Z.; Feng, J.; Yang, J. Record of the Environmental Change Since Holocene in the Region of Gongwang Moutain, Yunnan Province. *Earth Environ.* **2007**, *35*, 343–350.
60. Suttner, L.J.; Dutta, P. Alluvial Sandstone Composition and Paleoclimate, I. Framework Mineralogy. *J. Sediment. Res.* **1986**, *56*, 329–345. [CrossRef]
61. Elrick, M.; Reardon, D.; Labor, W.; Martin, J.; Desrochers, A.; Pope, M. Orbital-scale climate change and glacioeustasy during the early Late Ordovician (pre-Hirnantian) determined from δ18O values in marine apatite. *Geology* **2013**, *41*, 775–778. [CrossRef]
62. Dahl, T.W.; Hammarlund, E.U.; Rasmussen, C.M.Ø.; Bond, D.P.; Canfield, D.E. Sulfidic anoxia in the oceans during the Late Ordovician mass extinctions—Insights from molybdenum and uranium isotopic global redox proxies. *Earth-Sci. Rev.* **2021**, *220*, 103748. [CrossRef]
63. Kozik, N.P.; Gill, B.C.; Owens, J.D.; Lyons, T.W.; Young, S.A. Geochemical Records Reveal Protracted and Differential Marine Redox Change Associated With Late Ordovician Climate and Mass Extinctions. *AGU Adv.* **2022**, *3*, e2021AV000563. [CrossRef]
64. Bhatia, M.R.; Taylor, S.R. Trace-element geochemistry and sedimentary provinces: A study from the Tasman Geosyncline, Australia. *Chem. Geol.* **1981**, *33*, 115–125. [CrossRef]
65. Roser, B.P.; Korsch, R.J. Geochemical characterization, evolution and source of a Mesozoic accretionary wedge: The Torlesse terrane, New Zealand. *Geol. Mag.* **1999**, *136*, 493–512. [CrossRef]
66. Verma, S.P.; Rivera-Gómez, M.A.; Díaz-González, L.; Pandarinath, K.; Amezcua-Valdez, A.; Rosales-Rivera, M.; Verma, S.K.; Quiroz-Ruiz, A.; Armstrong-Altrin, J.S. Multidimensional classification of magma types for altered igneous rocks and application to their tectonomagmatic discrimination and igneous provenance of siliciclastic sediments. *Lithos* **2017**, *278–281*, 321–330. [CrossRef]
67. Liu, Z.; Algeo, T.J.; Guo, X.; Fan, J.; Du, X.; Lu, Y. Paleo-environmental cyclicity in the Early Silurian Yangtze Sea (South China): Tectonic or glacio-eustatic control? *Palaeogeogr. Palaeoclimatol. Palaeoecol.* **2017**, *466*, 59–76. [CrossRef]
68. Chen, X.; Chen, L.; Tan, X.; Jiang, S.; Wang, C. Impact of pyrite on shale gas enrichment—A case study of the Lower Silurian Longmaxi Formation in southeast Sichuan Basin. *Front. Earth Sci.* **2021**, *15*, 332–342. [CrossRef]
69. Farrell, Ú.C.; Samawi, R.; Anjanappa, S.; Klykov, R.; Adeboye, O.O.; Agic, H.; Ahm, A.-S.C.; Boag, T.H.; Bowyer, F.; Brocks, J.J.; et al. The Sedimentary Geochemistry and Paleoenvironments Project. *Geobiology* **2021**, *19*, 545–556. [CrossRef]
70. Men, X.; Mou, C.; Ge, X. Changes in palaeoclimate and palaeoenvironment in the Upper Yangtze area (South China) during the Ordovician-Silurian transition. *Sci. Rep.* **2022**, *12*, 13186. [CrossRef]
71. Shi, Z.; Zhao, S.; Zhou, T.; Ding, L.; Sun, S.; Cheng, F. Mineralogy and Geochemistry of the Upper Ordovician and Lower Silurian Wufeng-Longmaxi Shale on the Yangtze Platform, South China: Implications for Provenance Analysis and Shale Gas Sweet-Spot Interval. *Minerals* **2022**, *12*, 1190. [CrossRef]
72. Floyd, P.A.; Leveridge, B.E. Tectonic environment of the Devonian Gramscatho basin, south Cornwall: Framework mode and geochemical evidence from turbiditic sandstones. *J. Geol. Soc.* **1987**, *144*, 531–542. [CrossRef]
73. Nesbitt, H.W.; Wilson, R.E. Recent chemical weathering of basalts. *Am. J. Sci.* **1992**, *292*, 740–777. [CrossRef]
74. Allègre, C.J.; Minster, J.F. Quantitative models of trace element behavior in magmatic processes. *Earth Planet. Sci. Lett.* **1978**, *38*, 1–25. [CrossRef]
75. Roser, B.P.; Korsch, R.J. Provenance signatures of sandstone-mudstone suites determined using discriminant function analysis of major-element data. *Chem. Geol.* **1988**, *67*, 119–139. [CrossRef]
76. Zhang, G.; Guo, A.; Wang, Y.; Li, S.; Dong, Y.; Liu, S.; He, D.; Cheng, S.; Lu, R.; Yao, A. Tectonics of South China continent and its implications. *Sci. China Press* **2013**, *43*, 1553–1582. [CrossRef]
77. Shu, L.; Wang, B.; Cawood, P.A.; Santosh, M.; Xu, Z. Early Paleozoic and Early Mesozoic intraplate tectonic and magmatic events in the Cathaysia Block, South China. *Tectonics* **2015**, *34*, 1600–1621. [CrossRef]

78. Huang, H.; He, D.; Li, Y.; Li, J.; Zhang, L. Silurian tectonic-sedimentary setting and basin evolution in the Sichuan area, southwest China: Implications for palaeogeographic reconstructions. *Mar. Pet. Geol.* **2018**, *92*, 403–423. [CrossRef]
79. Jia, J.; Du, X.; Zhao, K.; Lu, Y.; Tan, C. Sources of K-bentonites across the Ordovician-Silurian transition in South China: Implications for tectonic activities on the northern and southern margins of the South China Block. *Mar. Pet. Geol.* **2022**, *139*, 105599. [CrossRef]
80. Xiao, B.; Xiong, L.; Zhao, Z.; Fu, X.; Zhao, Z.; Hou, H.; Liu, S. Late Ordovician-Early Silurian extension of the northern margin of the Upper Yangtze Platform (South China) and its impact on organic matter accumulation. *J. Pet. Sci. Eng.* **2023**, *220*, 111238. [CrossRef]
81. Shu, L.; Yu, J.; Jia, D.; Wang, B.; Shen, W.; Zhang, Y. Early Paleozoic Orogenic Belt in the Eastern Segment of South China. *Geol. Bull. China* **2008**, *27*, 1581–1593.
82. Xu, Y.; Cawood, P.A.; Du, Y.; Huang, H.; Wang, X. Early Paleozoic orogenesis along Gondwana's northern margin constrained by provenance data from South China. *Tectonophysics* **2014**, *636*, 40–51. [CrossRef]
83. Yao, W.; Li, Z. Tectonostratigraphic history of the Ediacaran–Silurian Nanhua foreland basin in South China. *Tectonophysics* **2016**, *674*, 31–51. [CrossRef]
84. Li, S.; Li, X.; Zhao, S.; Yang, C.; Liu, X.; Guo, L.; Wang, Y.; Hao, Y.; Zhang, J.; Hu, M. Global Early Paleozoic Orogens (III): Intracontinental Orogen in South China. *J. Jilin Univ. (Earth Sci. Ed.)* **2016**, *46*, 1005–1025. [CrossRef]
85. Bhatia, M.R. Plate Tectonics and Geochemical Composition of Sandstones. *J. Geol.* **1983**, *91*, 611–627. [CrossRef]
86. Roser, B.P.; Korsch, R.J. Determination of Tectonic Setting of Sandstone-Mudstone Suites Using SiO_2 Content and K_2O/Na_2O Ratio. *J. Geol.* **1986**, *94*, 635–650. [CrossRef]
87. Bhatia, M.R.; Crook, K.A.W. Trace element characteristics of graywackes and tectonic setting discrimination of sedimentary basins. *Contrib. Miner. Pet.* **1986**, *92*, 181–193. [CrossRef]
88. Verma, S.P.; Armstrong-Altrin, J.S. New multi-dimensional diagrams for tectonic discrimination of siliciclastic sediments and their application to Precambrian basins. *Chem. Geol.* **2013**, *355*, 117–133. [CrossRef]
89. Zhang, Q. Black Shale from the Longmaxi Formation in the Western Xikang-Yunnan Ancient Land: Geochemistry and Sedimentary. Ph.D. Thesis, Chengdu University of Technology, Chengdu, China, 2017.
90. Liu, C.; Xiong, G.; Dong, G.; Cui, W. Geochemical characteristics of mudstones and its provenance and tectonic setting during the Ordovician-Silurian period in northern margin of Yangtze Block. *Geol. Rev.* **2021**, *67*, 67040002.
91. Xiong, G.; Liu, C.; Dong, G.; Cui, W. A study of element geochemistry of mudstones of upper Ordovician Wufeng Formation and lower Silurian Longmaxi Formation in southern Daba Mountain. *Sediment. Geol. Tethyan Geol.* **2021**, *41*, 398–417. [CrossRef]
92. Li, Q.; Lan, B.; Li, G.; Xu, S.; Liu, T.; Gou, Q.; Wang, Y. Geochemical Characteristics of Element and Their Geological Significance of Wufeng-Longmaxi Formation Shales in North Margin of the Central Guizhou Uplift. *Earth Sci.* **2021**, *46*, 3172–3188.
93. Ge, X.; Mou, C.; Xu, Q.; Liu, W.; Men, X.; He, J.; Deng, B.; Liang, W. A study on the enrichment of organic materials in black shales of the Wufeng to Longmaxi Formations in eastern Sichuan Basin. *Sediment. Geol. Tethyan Geol.* **2021**, *41*, 418–435.
94. Zheng, Y.; Mou, C.; Wang, X. Sedimentary Geochemistry and Patterns of Organic Matter Enrichment of Wufeng-Longmaxi Formations in the Southern Margin of Sichuan Basin, China. *J. Earth Sci. Environ.* **2019**, *41*, 541–560.
95. Yang, G.; Xiu, Y.; Liu, J.; He, L.; Yang, H. Geochemical Characteristics and Their Significances of Black Shale of the Silurian Longmaxi Formation in the Leibo-Yongshan Region on the Southwestern Margin of the Sichuan Basin. *Acta Geol. Sichuan* **2019**, *39*, 670–678.
96. Jia, M. Shale Characteristics and Organic Matter Accumulation Mechanism of Wufeng-Longmaxi Formation in Northeastern Sichuan Basin. Master's Thesis, Lanzhou University, Lanzhou, China, 2019.
97. Zhang, N.; Lin, C.; Zhou, J.; Chen, S.; Liu, Y.; Dong, G. REE Characteristics of the 1st Member of Eocene Dainan Formation in Gaoyou Depression of North Jiangsu Basin, and Its Significance in Provenance Instruction. *Geol. Rev.* **2012**, *58*, 369–378.
98. Xu, Z.; Li, Y.; Ji, S.; Li, G.; Pei, X.; Ma, X.; Xiang, H.; Wang, R. Qinling gneiss domes and implications for tectonic evolution of the Early Paleozoic Orogen in Central China. *J. Asian Earth Sci.* **2020**, *188*, 104052. [CrossRef]